

Time-Dependent BPS Skyrmions

Theodora Ioannidou¹ and Árpád Lukács²

*Faculty of Civil Engineering, School of Engineering, Aristotle University of Thessaloniki,
Thessaloniki 54124, Greece*

Abstract

An extended version of the BPS Skyrme model that admits time-dependent solutions is discussed. Initially, by introducing a power law at the original potential term of the BPS Skyrme model the existence, stability and structure of the corresponding solutions is investigated. Then, the frequencies and half-lives of the radial oscillations of the constructed time-dependent solutions are determined.

1 Introduction

The classical Skyrme model [1] is a strong candidate for describing the low energy regime of quantum chromodynamics (for up-to-date research, see for example, Ref. [2]). The Skyrme model is a nonlinear theory of mesons in three space dimensions admitting as solutions topological solitons, the so-called skyrmions. Each skyrmion is associated with a topological charge, interpreted as baryon number n ; and therefore, skyrmions are baryons emerging from a meson field. Since its original formulation, the Skyrme model has been able to predict the nucleon properties up to thirty percent. Therefore, several modifications of the classical model have been considered aiming to improve the predictions.

One such modification was introduced in [3] by adding a sextic term (instead of a quartic one) in the classical Skyrme model Lagrangian, for stabilising the skyrmions. Alternatively, both terms can be retained. However, the latter can produce some problems since in the *non static case* the two time derivatives lead to pathological runaway solutions. This is not true in the *static case* as shown in [4], where the classical properties of a generalised Skyrme model by considering a combination of the quartic and sextic term have been studied. The

¹*Email:* ti3@auth.gr

²*Email:* arpadlukacs@civil.auth.gr

corresponding skyrmions were obtained following numerical techniques and approximations used in the classical case and it was shown that they possess the same symmetries as the classical ones but are more bound.

Recently in [5], a submodel of the generalised Skyrme model has been considered, which consists, *only*, of the square of the baryon current and a potential term. This model is called the BPS Skyrme model since a Bogomolny bound exists and the static solution saturates it. By choosing a particular type of the potential, the BPS Skyrme model admits topological compactons (solitons that reach the exact value at a finite distance; that is, with compact support) which can be obtained analytically and reproduce features and properties of the liquid drop model of nuclei (for details see, for example, Ref. [6] and references in it). However, most of the investigations have considered the static case since the BPS Skyrme model does not have a well defined Cauchy problem due to the non-standard kinetic term and the non-analytic behaviour of the compactons at the boundaries.

In this paper we consider the dynamics of the BPS Skyrme model and investigate the existence, stability and structure of time-dependent configurations. Initially, a generalised version of the potential is introduced. Then, the existence of the corresponding solitons is studied for different values of the parameter. In addition, it is shown how by varying the parameter the BPS skyrmions transform from solitons to compactons.

2 The BPS Skyrme Model

The action of the BPS Skyrme model is defined by

$$S = \int d^4x \{ -\lambda^2 \pi^2 B^\mu B_\mu - \mu^2 V(U, U^\dagger) \}, \quad (1)$$

where $U(t, \mathbf{x})$ is the Skyrme field (that is, an $SU(2)$ -valued scalar field); μ is a free parameter with units MeV^2 ; $V(U, U^\dagger)$ is the potential (or mass) term which breaks the chiral symmetry of the model; λ is a positive constant with units MeV^{-1} ; and B^μ is the topological current density defined by

$$B^\mu = \frac{1}{24\pi^2} \epsilon^{\mu\nu\rho\sigma} \text{tr} (L_\nu L_\rho L_\sigma), \quad (2)$$

where $L_\mu = U^\dagger \partial_\mu U$ is the $su(2)$ -valued current and $g_{\mu\nu} = \text{diag}(1, -1, -1, -1)$ is the Minkowski metric. Using scaling arguments it can be shown that the first term prevents the BPS skyrmions from shrinking to zero size while the potential term stabilizes them against arbitrary expansion. By construction, the BPS model is more topological in nature than the classical Skyrme model.

By rescaling $x^\mu \rightarrow (\lambda n / \sqrt{2\pi\mu})^{1/3} x^\mu$ where n being the baryon number, the action (1) becomes

$$S = -\frac{\mu^2}{2} \left(\frac{\lambda n}{\sqrt{2\pi\mu}} \right)^{4/3} \int d^4x \left\{ \frac{1}{144n^2} [\epsilon^{\mu\nu\rho\sigma} \text{tr}(L_\nu L_\rho L_\sigma)]^2 + 2V(U, U^\dagger) \right\}. \quad (3)$$

In what follows, we consider the action (3) divided by $(\lambda n / \sqrt{2\pi\mu})^{4/3}$.

Similarly to the classical case [7], we parametrize U by a real scalar field f and a three component unit vector $\hat{\mathbf{n}}$ as

$$U = \exp(i f \vec{\sigma} \cdot \hat{\mathbf{n}}) \quad (4)$$

where $\vec{\sigma} = (\sigma^1, \sigma^2, \sigma^3)$ are the Pauli matrices. The vector field is related to a complex scalar field ψ by the stereographic projection

$$\hat{\mathbf{n}} = \frac{1}{1 + |\psi|^2} (\psi + \bar{\psi}, -i(\psi - \bar{\psi}), 1 - |\psi|^2). \quad (5)$$

For simplicity, we consider spherical symmetry. This is done by separation of the radial and angular dependence of the fields. In particular, using the polar coordinates $(r, \theta, \phi) \in \mathbb{R}^3$ we assume that $f = f(r, t)$ and $\psi = \psi(\vartheta, \varphi) \equiv \tan\left(\frac{\vartheta}{2}\right) e^{in\varphi}$. Then, the action (3) simplifies to

$$S = 2\pi\mu^2 \int dt \int dr r^2 \left[\frac{\sin^4 f}{r^4} (\dot{f}^2 - f'^2) - 2V \right], \quad (6)$$

and the corresponding equation of motion becomes

$$\frac{\sin^4 f}{r^4} \left(\ddot{f} - f'' + \frac{2}{r} f' \right) + \frac{2 \sin^3 f \cos f}{r^4} (\dot{f}^2 - f'^2) + \frac{\partial V}{\partial f} = 0. \quad (7)$$

It can be easily observed that the form of the potential plays a critical role for the existence and type of the corresponding solutions. Let the potential to be given by the power law

$$\begin{aligned} V_\alpha &= \frac{1}{2} (2 - \text{tr} U)^\alpha \\ &= (1 - \cos f)^\alpha, \end{aligned} \quad (8)$$

where $\alpha \in \mathbb{R}$ is a free parameter. Then, for $\alpha = 1$ the BPS Skyrme model studied in [5, 6] is obtained. For $\alpha < 3$, the solutions are compactons with a non-analytical behaviour at the boundaries. Finally, for $\alpha \geq 3$ time-dependent skyrmions can be derived as it is shown in Section 4. The aforementioned solutions are similar in their properties, since topology predominates the type of the potential.

3 Static BPS Skyrmions

Let us concentrate on the static case, i.e., $f = f(r)$. Then, the energy (6) can be expressed as a sum of a square and a topological quantity. That is,

$$E = 4\pi \int dr r^2 \left[\left(\frac{\sin^2 f}{r^2} f' \pm \sqrt{2V} \right)^2 \mp \frac{\sqrt{2V} \sin^2 f}{r^2} f' \right]. \quad (9)$$

Since the last term is topological invariant, in each topological sector a minimum is obtained satisfying the Bogomolny-Prasad-Sommerfield (BPS) equation

$$f' = \mp \frac{\sqrt{2V} r^2}{\sin^2 f} \quad (10)$$

i.e., when the square term of (9) vanishes. Solutions of equation (10) can be obtained either analytically or numerically depending on the form of the potential. In what follows, we assume that the potential is given by equation (8) and investigate the type and form of the obtained solutions for different values of α .

In the simplest case where $\alpha = 1$, a closed form for the profile function (10) exists. The obtained solutions (with different winding numbers) are related to each other since by rescaling the coordinates the winding number n of the ansatz drops out of equation (10).

Next, let us keep α arbitrary and study the asymptotic behaviour of the solution (10). Since the potential vanishes for $f = 2n\pi$ for $n \in \mathbb{Z}$, we consider $f(0) = \pi$ and $f(\infty) = 0$. This choice of boundary conditions sets the baryon number equal to the winding number.

At spatial infinity, equation (10) takes the form

$$f^{2-\alpha} f' = \mp \frac{r^2}{2^{(\alpha-1)/2}}, \quad (11)$$

and its solution (for $\alpha \neq 3$) is given by

$$f(r)^{3-\alpha} = \mp \frac{1}{2^{(\alpha-1)/2}} \left[\left(1 - \frac{\alpha}{3}\right) r^3 + c \right]. \quad (12)$$

For $\alpha > 3$, the solution has a power law tail since $f(r) \propto r^{\frac{1}{1-\alpha/3}}$; while for $\alpha = 3$ it becomes exponentially localised since

$$f(r) \sim \exp\left(-\frac{r^3}{6}\right).$$

Finally, for $\alpha < 3$ a non-analytic behaviour at the boundary leads to compacton solutions since for $r < r_b$, the profile function (10) is given by

$$f(r) \sim (r_b - r)^\gamma [c_0 + c_1 (r - r_b) + \dots],$$

where

$$\gamma = \frac{1}{3 - \alpha}, \quad c_0 = \left[\sqrt{2} r_b^2 (3 - \alpha) \right]^\gamma, \quad c_1 = \sqrt{2} r_b c_0^{\alpha-2}.$$

Recall that, at the origin, the profile function of a regular solution is given by: $f = \pi + f'(0)r + \mathcal{O}(r^2)$.

The profile equation (10) of the aforementioned cases have been obtained numerically using Dormand–Prince 8th order Runge–Kutta integration with embedded error estimation and adaptive step size control [8]. The results are presented in Figure 1 which displays the solutions of (10) (with the minus sign) for different values of $\alpha \geq 3$. In addition, Figure 2 presents the total energy (9) and energy density \mathcal{E} (i.e., $E(R) = 4\pi \int_0^R dr r^2 \mathcal{E}$) for different values of α . Finally, Figure 3 displays the total energy (9) as a function of α .

4 Dynamics of BPS Skyrmions

Let us conclude by concentrating on the non static case. For $\alpha > 3$, the model has a well-defined dynamics since the principal part of the differential equation (7), $\ddot{f} - f''$, is the same as that of the Klein-Gordon one.

To study the radial excitations of the BPS skyrmions we describe the soliton oscillations by collective coordinates [9, 10]. In particular, the radial pulsations are imposed due to the

α	E	K	U_1	U_2	ω_P
4	69.789	19.066	34.894	34.894	3.314
5	81.711	17.632	40.850	40.850	3.728
6	97.731	16.603	48.851	48.851	4.202
7	118.881	15.863	59.417	59.417	4.741
8	146.611	15.340	73.275	73.275	5.354
9	182.892	14.987	91.411	91.411	6.049
10	230.371	14.772	115.148	115.148	6.839

Table 1: Numerical data of the static solution for different values of α .

variational ansatz

$$f(r, t) = f_0 \left(\frac{r}{\rho(t)} \right), \quad (13)$$

where f_0 is the static profile function by setting $r \rightarrow r/\rho(t)$. Then the action (6) takes the form

$$L_\rho = K \frac{\dot{\rho}^2}{\rho^3} - U_1 \frac{1}{\rho} + U_2 \rho^3, \quad (14)$$

where K , U_1 , U_2 are defined by the integrals

$$\begin{aligned} K &= 4\pi \int dr \sin^4 f_0 f_0'^2, \\ U_1 &= 4\pi \int dr \frac{\sin^4 f_0}{r^2} f_0'^2, \\ U_2 &= 8\pi \int dr r^2 V(f_0). \end{aligned} \quad (15)$$

For small oscillations, L_ρ needs to be expanded up to second order around $\rho = 1$. Then the first order term vanishes (that is, $U_1 = U_2$) since f_0 is a solution of the static field equations; while the second order term is equal to the Lagrangian of a harmonic oscillator with frequency

$$\omega_P^2 = \frac{6 U_2}{K}. \quad (16)$$

The precision of the predicted frequencies deteriorates as α increases. That happens because as α increases the tail of the oscillation becomes predominant and thus, the shape of the solution changes. In Table 1, the values of the constants K_1 , U_1 , U_2 and the oscillation

frequencies ω_P are given for different values of α . The vanishing of the first order term of the Lagrangian (that is, $U_1 = U_2$) verifies the precision of our numerics.

For the numerical simulations, equation (7) is discretised on a uniform grid in space and time. In particular, for the spatial coordinate, a second order finite difference discretisation and for the time coordinate, the fourth order Runge-Kutta method (method of lines [11]) have been considered. The default grid size is $r = [0 \dots 20]$ and $t = [0 \dots 10]$ with 8×10^3 spatial and 10^4 temporal grid points (due to Courant stability criterion). The accuracy of the results have been verified by running simulations on a longer radial interval and half step sizes.

In addition, the Neumann boundary conditions at large r have been applied. As initial data a uniformly stretched skyrmion has been used. Then, the frequencies and the decay constants of the oscillation modes have been measured; verifying that they are independent of the amplitude of the stretch and the parameters of the simulation. For large values of time ($t > 1$) and given r (inside the soliton core, e.g., $r = 0.05$), the decaying oscillations are approximated by $f(x, t) - f_0(x) \approx A_x \cos(\omega t + \delta) / 2^{t/T}$. Then, for the interval $t = 1 \dots 7$, the amplitude A_x , the frequency ω and the half-life T are obtained (with below 1% precision) by a least squares fit. In Table 2, the frequencies and half-lives of the deformed skyrmion oscillations are presented and compared with the one (that is, ω_P) obtained from the collective coordinate approximation. Note that, there is a difference between the measured frequencies and the ones obtained by the uniform oscillation approximation [10]. This is explained by studying the time evolution of the deformed skyrmions. As demonstrated in Figure 4, in the interior of the skyrmion the deformation (described by the continues line) is a genuine pulsation while in the exterior the deformation (described by the dashed line) is a wave packet travelling outwards.

Finally, we investigate the time evolution of small perturbations (of a Gaussian form) as they travel with different velocities towards or away from the skyrmion. Time snapshots of these oscillations are presented in Figures 5 and 6. As it can be seen the perturbation initially travels towards the skyrmion then stops by spreading the wave packet, and finally dominates. As the wave travels outward, its wavelength and amplitude increases, until it is

a	ω_P	ω	T
4	3.314	3.34	5.17
5	3.728	3.90	1.46
6	4.202	4.71	0.83
7	4.741	5.64	0.58
8	5.354	6.69	0.44
9	6.049	7.90	0.34
10	6.839	9.28	0.28

Table 2: Frequencies and half-lives of oscillations of deformed skyrmions.

stopped due to nonlinearities. This should be expected since the linearized field equation has no solutions with scattering asymptotics.

5 Conclusions

By modifying the potential term of the BPS Skyrme model, the non-compact static soliton solutions are well-defined and sufficiently well-behaved in the whole space; while the corresponding equation (7) is well-defined for sufficiently small fluctuations about a static soliton and for sufficiently small time intervals. Also, the spherically symmetric sector of the dynamics of the model has been implemented numerically and time-dependent solutions that correspond to radial pulsation and propagations of disturbances have been derived. The significance of the chosen potential is based on the fact that the corresponding solutions are not compactons; that is, have analytic behaviour at the boundaries.

As a next step, the investigation of the scattering of two BPS skyrmions is going to be considered. In this case, the initial conditions consist of two separated static solutions, Lorentz boosted with opposite velocities. Due to lack of obvious symmetries, one needs to solve the full three-dimensional equation numerically. We hope to report on this issue soon.

Acknowledgements

T.I. thanks Christoph Adam for useful discussions.

T.I. acknowledges support from FP7, Marie Curie Actions, People, International Research Staff Exchange Scheme (IRSES-606096). T.I. and Á.L. acknowledge support from The Hellenic Ministry of Education: Education and Lifelong Learning Affairs, and European Social Fund: NSRF 2007-2013, Aristeia (Excellence) II (TS-3647).

References

- [1] T.H.R. Skyrme, Proc. Roy. Soc. London A. 260 (1961) 127; 262 (1961) 237; Nucl. Phys. 31 (1962) 556.
- [2] D. Foster and N.S. Manton, Nucl. Phys. B 899 (2015) 513; C.J. Halcrow and N.S. Manton, JHEP 1501 (2015) 016 ; P.H.C. Lau and N.S. Manton, Phys. Rev. Lett. 113 (2014) 23; Phys. Rev. D 89 (2014) 12.
- [3] A. Jackson, A.D. Jackson, A.S. Goldhaber, G.S. Brown and L.C. Castillo, Phys. Lett. B 154 (1985) 101.
- [4] L. Marleau, Phys. Lett. B 235 (1990) 141; Phys. Lett. B 244 (1990) 580; I. Floratos and B. Piette, J. Math. Phys. 42 (2001) 5580; Phys. Rev. D 64 (2001) 045009.
- [5] C. Adam, P. Klimas, J. Sanchez-Guillen, and A. Wereszczynski, J. Math. Phys. 50 (2009) 022301.
- [6] C. Adam, J. Sanchez-Guillen, and A. Wereszczynski, Phys. Lett. B 691 (2010) 105; Phys. Rev. D 82 (2010) 085015; C. Adam, C. Naya, J. Sanchez-Guillen, and A. Wereszczynski, Phys. Rev. Lett. 111 (2013) 232501; C. Adam, C.D. Fosco, J.M. Queiruga, J. Sanchez-Guillen, and A. Wereszczynski, J. Phys. A: Math. Theor. 46 (2013) 135401.
- [7] C. Houghton, N. Manton and P. Sutcliffe, Nucl. Phys. B 510 (1998) 587; T. Ioannidou, B. Piette and W. J. Zakrzewski, J. Math. Phys. 40 (1999) 6353; J. Math. Phys. 40 (1999) 6223.

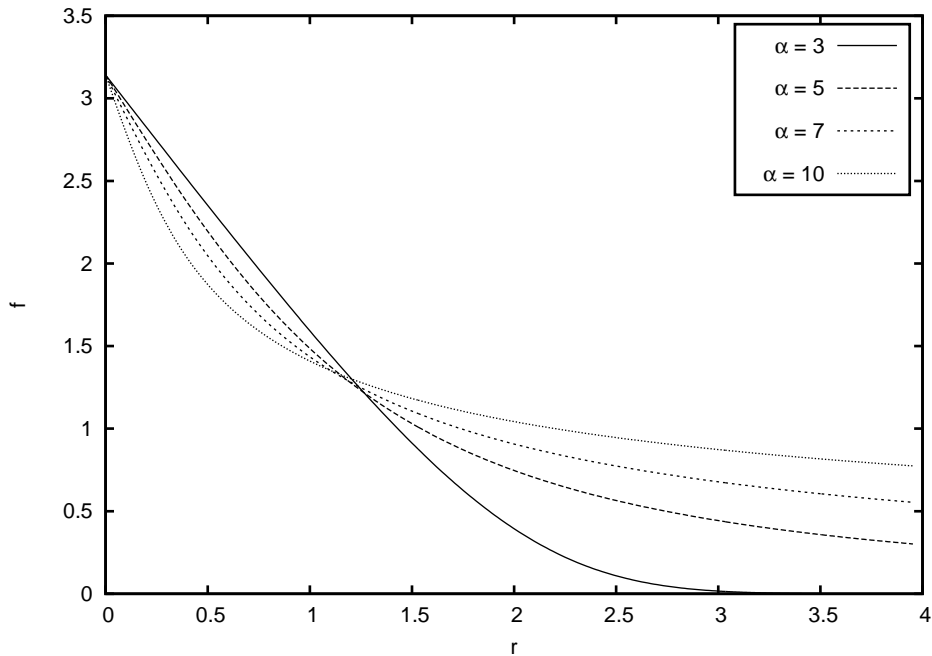


Figure 1: The profile function given by (10) for different values of α .

- [8] W.H. Press, S.A. Teukolsky, W.T. Vetterling, and B.P. Flannery, *Numerical Recipes 3rd Edition: The Art of Scientific Computing*, CUP (2007).
- [9] M.J. Rice, Phys. Rev. B 28 (1983) 3587.
- [10] C. Adam, C. Naya, J. Sanchez-Guillen, and A. Wereszczynski, Phys. Lett. B 726 (2013) 892.
- [11] W.E. Schiesser, *The Numerical Method of Lines: Integration of Partial Differential Equations*, Academic Press (1991).

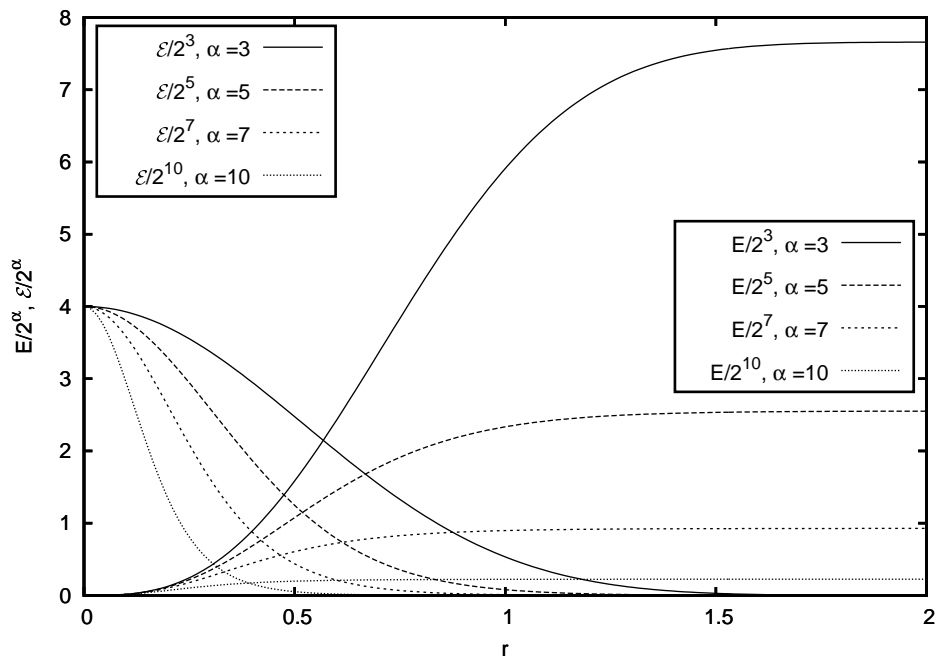


Figure 2: The total energy and energy density given by (9) for different values of α .

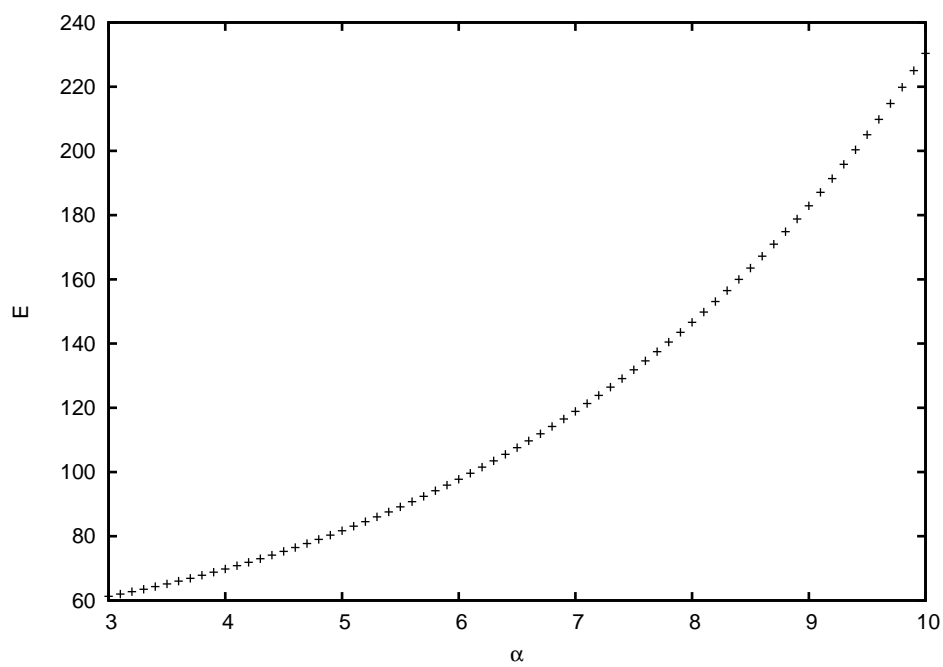


Figure 3: The total energy (9) as a function of α .

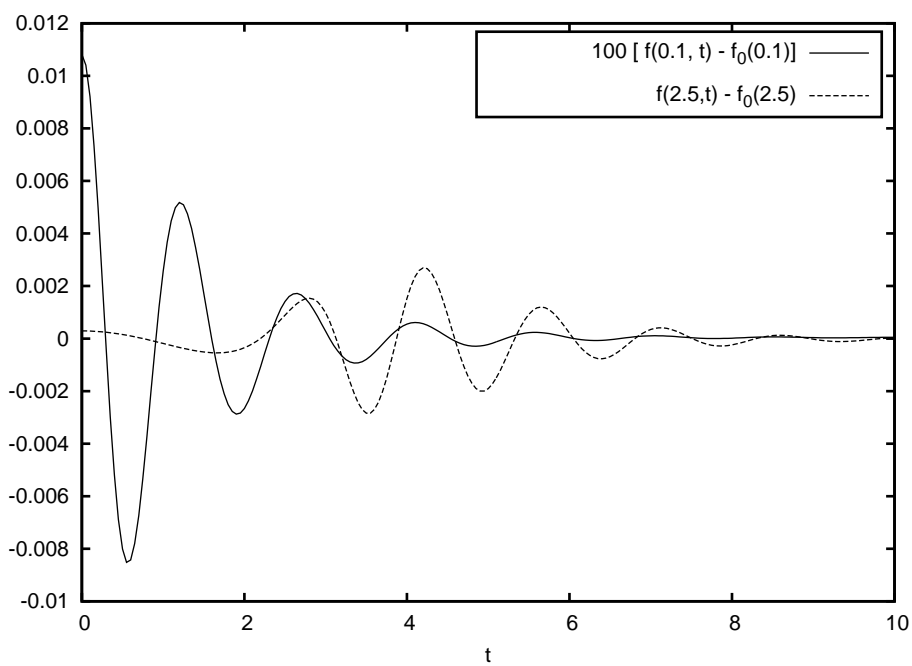


Figure 4: Time evolution of an oscillating skyrmion with initial stretching 0.05% and $\alpha = 6$, at two different points.

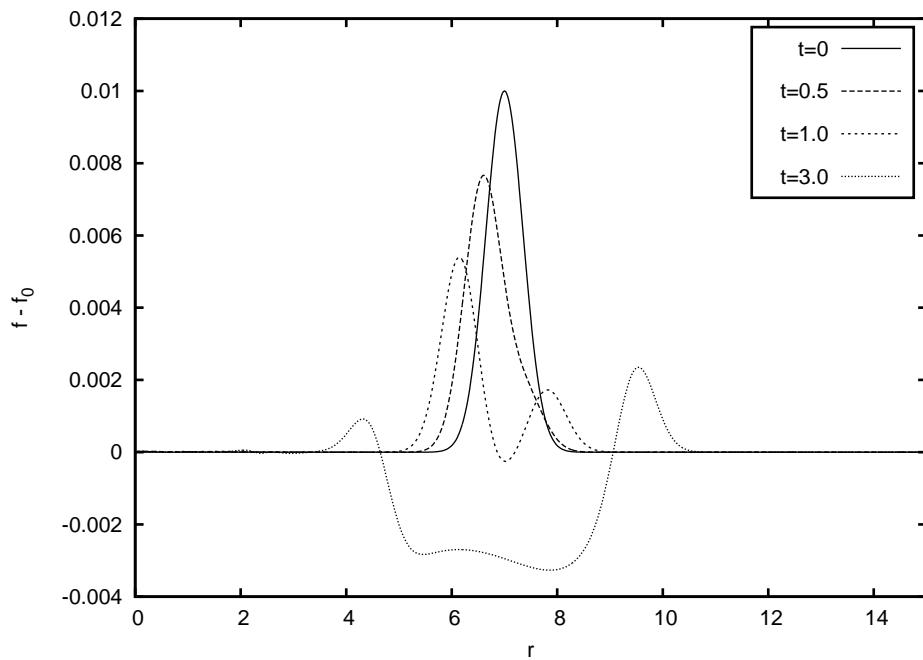


Figure 5: Time evolution of a small perturbation on a skyrmion when $\alpha = 6$. The amplitude of the initial Gaussian is 0.01, its velocity -0.8 (moving in), its squared width 0.25 and it is centered at $r = 7$.

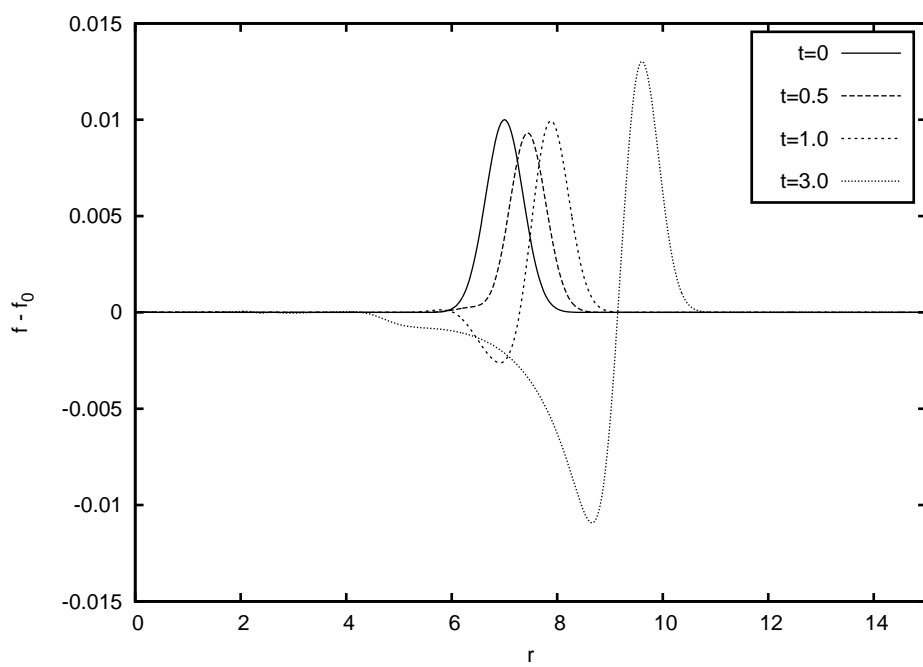


Figure 6: Same as Figure 5 but with the wave moving out with velocity 0.8.